RSC Advances

PAPER

View Article Online
View Journal | View Issue

Cite this: *RSC Adv.*, 2016, **6**, 91209

In situ preparation of multi-wall carbon nanotubes/Au composites for oxygen electroreduction†

Na Li,[ab] Zhenghua Tang,*[ac] Likai Wang,[a] Qiannan Wang,[a] Wei Yan,[a] Hongyu Yang,[a] Shaowei Chen[ad] and Changhong Wang*[b]

Received 27th June 2016
Accepted 16th September 2016

DOI: 10.1039/c6ra16533h

www.rsc.org/advances

Multi-wall carbon nanotubes (CNTs)/Au nanocomposites have been prepared by the *in situ* reduction approach. The as-prepared hybrid materials were characterized by X-ray diffraction (XRD), X-ray photoelectron spectroscopy (XPS) and transmission electron microscopy (TEM). The composition of the nanocomposites was fine tuned by varying the mass ratio of Au-to-CNTs. Among a series of samples tested, hybrid materials with a Au/carbon nanotubes (Au/CNTs) ratio = 1 : 2 demonstrated the best activity towards oxygen reduction reaction (ORR), as most positive onset potential, largest kinetic current density, highest amount of electron transfer and lowest H_2O_2 yields were obtained. Notably, the Au/CNTs also exhibited remarkable long-term durability higher than commercial Pt/C.

Introduction

A proton exchange membrane fuel cell (PEMFC) has been considered one of the most promising technologies to tackle the global energy crisis and environmental problems.[1,2] Oxygen reduction reaction is a key process for energy conversion in fuel cells, unfortunately, the slow reaction kinetics of ORR as well as the high price of the Pt based catalysts significantly hinder the widespread commercialization of fuel cells.[3,4] Moreover, the Pt based catalysts also suffer from the low abundance of Pt on earth as well as the poor stability of such catalysts. Therefore, a great deal of research efforts have been continuously devoted to developing new strategies to lower the amount of Pt or substituting Pt with other non-precious metals or even using metal-free materials.[5–15]

Bulk gold has been considered to be catalytically inert previously for a long time. However, when the dimension reaches nanometer scale, gold nanoparticles demonstrated excellent catalytic activity in multiple organic reactions[16] and electrochemical reaction. Particularly, for those ultrasmall nanoclusters with core diameter less than 2 nm, excellent activity toward oxygen electroreduction was observed by Chen's group.[17] Interestingly, strong size effects were observed and the activity increased with the decreasing of the core size. Smaller sized particles possess higher fraction of low-coordinated surface atoms,[18,19] which can facilitate the oxygen adsorption on the surface and making them easily activated.

However, when employing gold nanoparticles or clusters alone for catalyzing electrochemical process, the surface ligands may block some active sites hence detrimental to the mass transport behaviors and electron transfer kinetics,[20] meanwhile, gold nanoparticles tend to aggregate, dissolve, sinter or decompose during the electrochemical reaction.[21] To conquer these issues, a variety of substrates including porous carbon,[22] carbon nanosheets,[23] carbon nanotubes,[24] TiO_2 [25] as well as other materials[26] have been employed as supports to stabilize or entrap the gold nanoparticles. For instances, Alexeyeva *et al.* found that glassy carbon electrode modified by gold nanoparticle (AuNP)/multi-walled carbon nanotubes (MWCTs) possessed effective ORR activity in acidic media, and a two-electron reduction pathway was taken.[27] By employing layer-by-layer deposition technique, nanocomposite catalysts of AuNP/PDDA-MWCTs were synthesized and enhanced activity was acquired.[28] Interestingly, the hybrid materials of AuNP/MWCTs can also be prepared by sputter deposition of gold on MWCTs followed by heat-treatment.[29]

To enhance the activity, these hybrid materials were generally subjected to pyrolysis or elevated temperature calcination to remove the surface ligands. Note that, these processes normally require high energy input and sophisticated sample preparation procedures. Surfactant-free Au nanoclusters in graphene

[a]*New Energy Research Institute, School of Environment and Energy, South China University of Technology, Guangzhou Higher Education Mega Centre, Guangzhou, 510006, P. R. China. E-mail: zhht@scut.edu.cn*

[b]*School of Materials and Energy, Guangdong University of Technology, Guangzhou, 510006, P. R. China. E-mail: wangchh@gdut.edu.cn*

[c]*Guangdong Provincial Key Laboratory of Atmospheric Environment and Pollution Control, Guangdong Provincial Engineering and Technology Research Center for Environmental Risk Prevention and Emergency Disposal, School of Environment and Energy, South China University of Technology, Guangzhou Higher Education Mega Centre, Guangzhou, 510006, China*

[d]*Department of Chemistry and Biochemistry, University of California, 1156 High Street, Santa Cruz, California 95064, USA*

† Electronic supplementary information (ESI) available: TEM images of CNTs, HR-TEM images of the Au/CNTs = 1 : 2 composite, additional linear scanning voltammetric (LSV) curves, and repeated LSV measurements of the Au/CNTs = 1 : 2 composite. See DOI: 10.1039/c6ra16533h

were prepared by Tang and coworkers, and the nanoclusters exhibited remarkable catalytic activity towards ORR.[30] Although much progress has been achieved on supported gold nanoparticles for ORR, to date, few examples have been reported regarding ligand-free gold nanoparticles prepared without high-temperature treatment for ORR. This is the main motivation of our current investigation.

Herein, we report the *in situ* formation of Au nanoparticles on the surface of multi-wall carbon nanotubes. The as-prepared hybrid materials were fully characterized by XRD, XPS and TEM. The composition of the nanocomposites was tuned by varying the mass ratio of Au-to-CNTs. Among a series of samples tested, hybrid materials with Au/CNTs = 1 : 2 demonstrated the best activity for ORR, in terms of onset potential, kinetic current density as well as long-term durability.

Experimental section

Materials

Hydrogen tetrachloroauric acid (III) trihydrate ($HAuCl_4 \cdot 3H_2O$, 98%, Energy Chemicals, Shanghai), sodium borohydride ($NaBH_4$, 98%, Aladdin industrial Corporation, Shanghai), Pt/C (20 wt%, Alfa Aesar), multiwall carbon nanotubes solution (9–10 wt%, Aladdin industrial Corporation, Shanghai), Nafion (99%, Alfa Aesar), water was supplied by a Barnstead nanopure water system (18.3 MΩ cm). All the chemicals and solvents were used as received.

In situ preparation of Au/CNTs composites

The Au/CNTs nanocomposites were prepared by a *in situ* reduction method. Briefly, 2 mL of 0.5 M $HAuCl_4 \cdot 3H_2O$ and 4 mL of 1 mg mL^{-1} aqueous dispersion of carbon nanotubes were mixed in a 25 mL round-bottom flask. The mass ratio of Au-to-CNTs was 1 : 2. The mixture was stirred for half an hour at room temperature. Then, 2 mL of 0.026 M $NaBH_4$ aqueous solution was added rapidly under vigorously stirring. The reaction was proceeded for half an hour, and the composite solution was obtained. The impurities in the solution were removed by centrifugation with de-ionized water. The composite catalyst solid powder was obtained by freezing drying for 24 h. Samples with other mass ratios were also prepared in a similar manner, of which the mass ratios of Au-to-CNTs were 1 : 4, 1 : 1 and 2 : 1, respectively.

Characterizations

The composition and microstructure of the composite catalysts were examined by XPS, XRD and TEM tests. For high-resolution (HR) TEM tests, the samples were dispersed in absolute ethanol, and dropcast directly onto a copper grid coated with a holey carbon film. The XRD patterns were obtained with the Bragg angle (2θ) changes in the scope of 10–90 degrees at room temperature by using Bruker D8 diffraction and Cu K alpha radiation ($\lambda = 0.1541$ nm). The XPS analysis was conducted with a VG MultiLab 2000 instrument with a monochromatic Al K X-ray source (Thermo VG Scientific).

Electrochemical measurements

The electrochemical tests were performed on a electrochemical workstation with CHI 750E (CH instruments Inc.) in 0.1 M KOH solution at room temperature. The platinum wire electrode and a Ag/AgCl electrode worked as the counter electrode and the reference electrode, respectively. The working electrode was a glassy carbon rotating ring disk electrode (37% collection efficiency) from the PINE instruments. Prior to use, the working electrode was cleaned with 0.3 μm alumina powder on a polishing mica cloth (CH instruments Inc.).

Typically, 1 mg catalyst was dispersed in 0.5 mL of anhydrous ethanol solution, and 5 μL 5 wt% Nafion was added into the mixture and sonicated for at least half an hour. 10 μL mixed liquor was dropcast onto the glassy carbon electrode and dried at room temperature. The loading capacity of all catalyst samples on the electrode surface was 80.8 μg cm^{-2}. In all tests, the Ag/AgCl reference electrode was calibrated with respect to a reversible hydrogen electrode (RHE). The cyclic voltammograms (CV) were conducted at a scan rate of 10 mV s^{-1}. $E_{RHE} = E_{Ag/AgCl} + 0.966$ V. Chronoamperometric responses were recorded in an O_2-saturated 0.1 M KOH solution at +0.5 V for 30 000 s.

Results and discussion

The morphology and surface structure of the as-prepared Au/CNTs composites were first examined by TEM measurements. The typical TEM images of carbon nanotubes can be found in Fig. S1.† Fig. 1 presents the representative TEM images of the nanocomposites and their corresponding size distribution histograms. One can see that, with lower gold mass loadings such as the samples of Au/CNTs (1 : 4 and 1 : 2), all the particles were dispersed onto CNTs without aggregation. The representative HR-TEM images of Au/CNTs (1 : 2) sample can be found in Fig. S2,† and well-defined particles with high crystalline were observed. However, with higher gold mass loading such as the samples of Au/CNTs (1 : 1 and 2 : 1), apparent aggregation phenomenon can be observed, and large bulky materials formed especially for the sample of Au/CNTs (2 : 1). Based on more than 100 counts of individual particles, the average diameter was calculated as 9.2 ± 2.3 nm, 9.7 ± 4.5 nm, 23.2 ± 9.6 nm and 60.8 ± 9.8 nm for the sample of 1 : 4, 1 : 2, 1 : 1 and 2 : 1, respectively.

Further structural insights regarding this series of nanocomposites were obtained by XRD and XPS measurements. As depicted in Fig. 2a, two peaks at $2\theta = 25.9°$ and 42.9° can be found, which can be ascribed to (002) and (101) hexagonal carbon crystal face (jcpds 75-1621), respectively. For Au/CNTs composites, four additional diffraction peaks can be easily identified at $2\theta = 38.3$, 44.5, 64.6, 77.6, which correspond well with (111), (200), (220), (311) diffraction of fcc gold.[31] Such results suggest that the Au nanoparticles were well incorporated into the CNTs. Consistent results can be found in the XPS tests in Fig. 2b. Besides the C1s peak at 284.3 eV and O1s peak at 531.4 eV from CNTs, additional peaks from Au (Au4d, 353.1 eV and 334.8 eV, Au4f, 83.2 eV) with strong signals can be easily identified. For all the nanocomposites, two peaks with strong

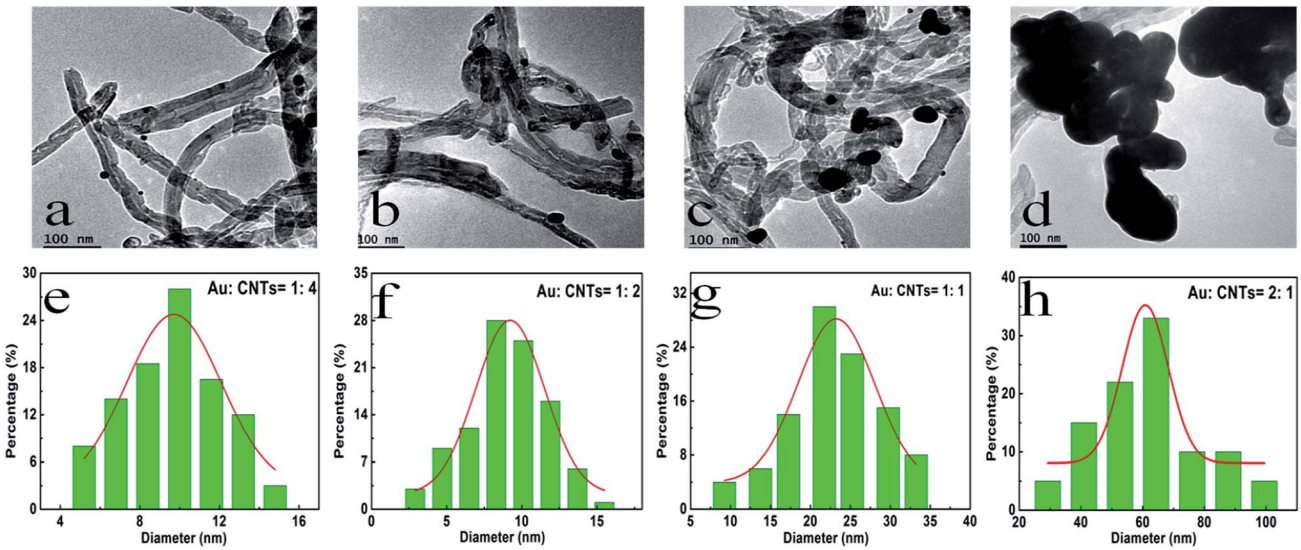

Fig. 1 Representative TEM images and corresponding size distribution histograms of (a, e) Au/CNTs = 1 : 4, (b, f) Au/CNTs = 1 : 2, (c, g) Au/CNTs = 1 : 1, and (d, h) Au/CNTs = 2 : 1.

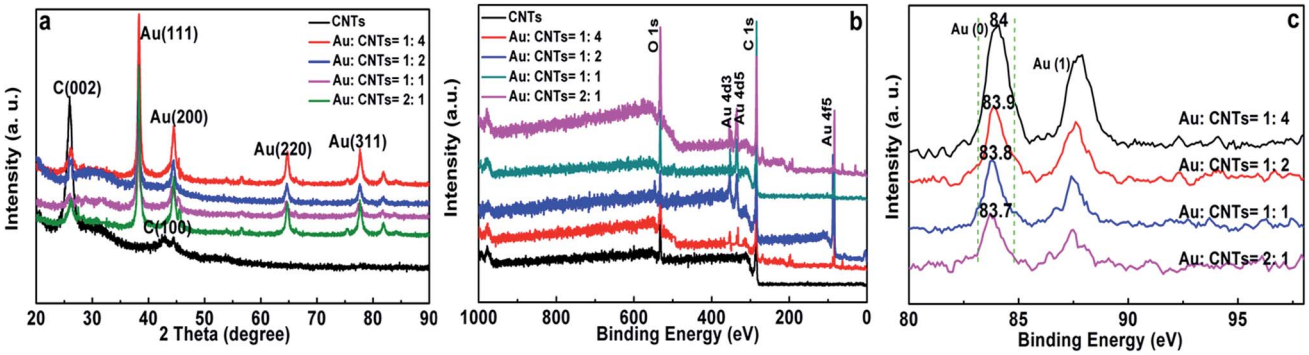

Fig. 2 (a) XRD patterns and (b) XPS survey spectra and (c) XPS Au4f core-level spectra of the Au/CNTs nanocomposites.

signal at ~87.5 eV and ~83.8 eV can be easily recognized, which are attributed to the binding energy of $Au4f_{5/2}$ and $Au4f_{7/2}$ electrons, respectively. The Au4f XPS spectra of the samples with different Au loadings were presented in Fig. 2c. It can be seen that, the binding energy of the $Au4f_{5/2}$ electrons decreased from 84.0 eV of Au/CNTs = 1 : 4 sample to 83.7 eV of Au/CNTs = 2 : 1 sample, in proportion with the gold mass loading decreasing. The blue shift of the binding energy indicates that covalent hybrid materials of Au/CNTs were obtained.[23–26] It is worth noting that such hybridization caused electronic interaction has been documented to facilitate the electron transfer kinetics and mass transport behaviors during the ORR process.[23–26,30] In addition, as shown in Fig. S3† of the Raman spectra, the intensity ratio of D/G band (I_d/I_G) of Au/CNTs = 1 : 2 (0.99) is much larger than that of CNTs alone (0.63). The higher I_d/I_G value of the hybrid materials further confirmed the strong interaction between Au elements and the CNTs support.[30]

Next, the ORR activities of these nanocomposites were examined by CV and rotating ring disk electrode (RRDE) tests. As seen in Fig. 3a, in oxygen-saturated 0.1 M KOH solution, a sharp cathodic peak attributed to oxygen reduction can be easily recognized, while in nitrogen-saturated 0.1 M KOH solution, only featureless charging currents were observed in the potential range from −0.03 V to +1.17 V, which can be seen in Fig. S4.† Among the series of samples, the nanocomposites with Au/CNTs (1 : 2) possessed the most positive onset potential, cathodic peak potential and largest kinetic current density, superior than carbon nanotubes and other samples as well. The onset potential and kinetic current densities (at +0.55 V and 2500 rpm) can be estimated to 0.79 V and 1.4 mA cm^{-2} for Au/CNTs (1 : 4), 0.86 V and 2.6 mA cm^{-2} for Au/CNTs (1 : 2), 0.71 V and 1.7 mA cm^{-2} for Au/CNTs (1 : 1), 0.72 V and 1.85 mA cm^{-2} for Au/CNTs (2 : 1) and 0.69 V and 1.39 mA cm^{-2} for CNTs, respectively. The Au/CNTs (1 : 2) sample possessed the best ORR activity among the series, which were further confirmed by the following RRDE measurements shown in Fig. 3b. It can be observed that for all the samples, when the electrode potential was scanned to ~0.7 V, non-zero cathodic currents started to appear and reached an plateau at ~0.5 V. In addition, the voltammetric current of the ring electrode was about one order of magnitude lower than that of the disk electrode, suggesting that a considerably small amount of hydrogen peroxide product was

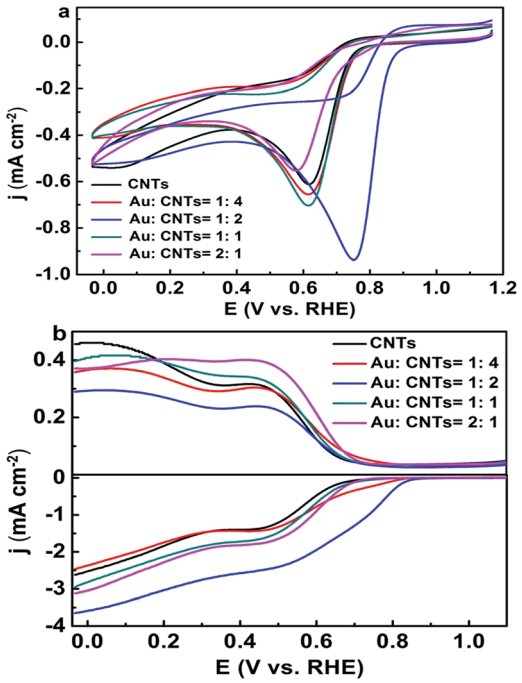

Fig. 3 CV (a) and RRDE (b) voltammograms of catalysts with different Au loadings in O_2-saturated 0.1 M KOH at 2500 rpm.

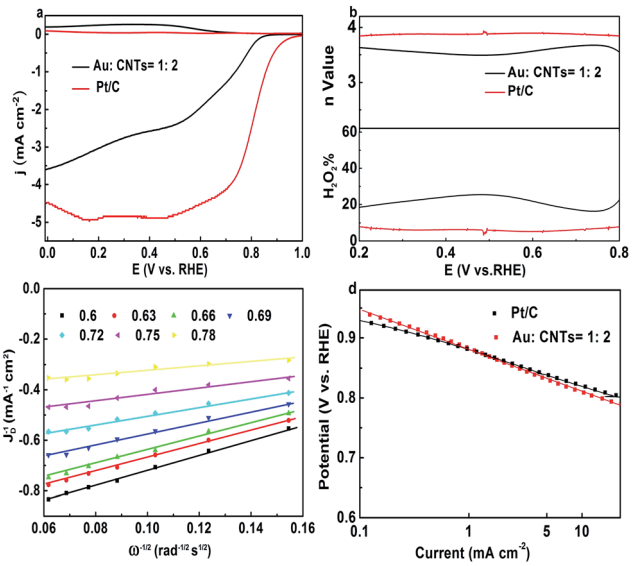

Fig. 4 (a) RRDE voltammograms at the 2500 rpm, (b) plots of H_2O_2 yield and number of electron transfer of a glassy carbon electrode modified with nanocomposite of Au/CNTs (1 : 2) in O_2-saturated 0.1 M KOH solution. Statistic results were based on data of three repeated measurements. (c) The corresponding K–L plots for nanocomposite of Au/CNTs (1 : 2) at different potentials. (d) The corresponding Tafel plots for nanocomposite of Au/CNTs (1 : 2) and commercial Pt/C catalyst. All measurements were conducted at a catalyst loading of 80.8 μg cm^{-2} in an O_2 saturated 0.1 M KOH aqueous solution with a sweep rate of 10 mV s^{-1}.

produced during the ORR. The catalyst performance varied with the change of Au-to-CNTs mass ratio. The huge variation between the catalytic performance with different Au loadings indicated a subtle balance between the gold content and the effective surface area. In principle, the number of electrocatalytic active sites increased with the increasing of the Au loading, and this is why the performance of Au/CNTs = 1 : 2 was better than that of Au/CNTs = 1 : 4. However, if $HAuCl_4$ was overloaded at the initial stage of synthesis (*e.g.* the sample of Au/CNTs = 2 : 1), aggregation as-prepared gold nanoparticles occurred and bulky materials were formed, evidenced by TEM images observed in Fig. 1d. The aggregation block some active sites hence significantly lower the ORR activity.

The electrocatalytic activities toward the ORR of the nanocomposites were then compared with Pt/C by the RRDE voltammetric method. The RRDE voltammetric measurements in Fig. 4a shows that the onset potential of Au/CNTs (1 : 2) and Pt/C were 0.85 V and 0.96 V, while the diffusion limited current density of Au/CNTs (1 : 2) and Pt/C was 2.64 and 4.80 mA cm^{-2} at 0.45 V and 2500 rpm, respectively.

According to the results of RRDE tests, the electron transfer number (n) and the yield of H_2O_2 in oxygen reduction process can be calculated by eqn (1) and (2):

$$n = \frac{4I_d}{I_d + I_r/N} \quad (1)$$

$$H_2O_2 = \frac{200I_r/N}{\frac{I_r}{N} + I_d} \quad (2)$$

in which, I_d is the disk current, I_r is the ring current, N is the collection efficiency of RRDE with a value of 0.37. As can be seen from Fig. 4b, for the nanocomposite of Au/CNTs (1 : 2), in the potential range from +0.2 V to +0.8 V, the n value varied from 3.50 to 3.69, while the H_2O_2 yield changed from 16.6% to 25.0%, both of which were close to the n (n = 3.70–3.86) and H_2O_2 yield of Pt/C (5.0% to 8.4%). It indicated that the reaction was a four electron process, with a small amount of intermediate product H_2O_2.

Fig. S5† presents the RRDE result of oxygen reduction for nanocomposite of Au/CNTs (1 : 2) collected with different rotation rates (from 100 to 2500 rpm) in the oxygen-saturated 0.1 M KOH solution. Clearly, as the rotation rates increased, the voltammetric current also increased. Fig. S4† presents the RRDE result of oxygen reduction for nanocomposite of Au/CNTs (1 : 2) collected with different rotation rates (from 100 to 2500 rpm) in the oxygen-saturated 0.1 M KOH solution. Clearly, as the rotation rates increased, the voltammetric current also increased. Under steady state conditions, the Koutecky–Levich (K–L) eqn (3) can express the relative contribution of kinetics and mass transport to the current generated in a RRDE measurement:[32]

$$\frac{1}{i} = \frac{1}{i_k} + \frac{1}{i_{l,c}} = \frac{1}{i_k} + \frac{1}{0.62nFAD_O^{2/3}\omega^{1/2}\nu^{-1/6}C_O^*} \quad (3)$$

where i is the measured current density, i_K and $i_{l,c}$ are the kinetic and diffusion limited current density, respectively, ω is the angular velocity of the disk (rad s^{-1}), F is the Faraday

constant, A is the cross sectional area of GC electrode (0.196 cm^2), C_O is the bulk concentration of dissolved O_2 (1.21×10^{-6} mol cm^{-3}), D_O is the diffusion coefficient of O_2 in 0.1 M KOH (1.93×10^{-5} cm^2 s^{-1}), and v is the kinematic viscosity of the electrolyte solution (0.01 cm^2 s^{-1}). Therefore, at potentials where mass transport and kinetics effects are dominant, a plot of I^{-1} *versus* $\omega^{-1/2}$ should be linear. Indeed, the corresponding K–L plots in Fig. 4c exhibited a good linearity within the potential range from 0.6 V to 0.78 V with rotation rate from 400 to 2500 rpm.

Furthermore, based on the K–L plots, the electron transfer number n can also be obtained from eqn (3). The n value of Au/CNTs = 1 : 2 was determined as 3.61, which is in good accordance with the n value range of 3.50 to 3.69 that obtained from RRDE measurements, suggesting a first order reaction kinetics of ORR with regard of the oxygen concentration. Fig. 4d shows the corresponding Tafel plots for nanocomposite of Au/CNTs (1 : 2) (red curve) (57.8 mV dec^{-1}) and Pt/C (black curve) (58 mV dec^{-1}). The two slopes were almost identical, which implied that they probably exhibited a similar reaction mechanism on the catalyst surface. Note that for Pt/C catalyst, the first electron transfer to molecular oxygen has been well recognized as the rate determining step in the ORR process.[33,34] Interestingly, such Tafel slope value of Au/CNTs (1 : 2) also agrees well with recently reported Au/C catalysts prepared by Erikson *et al.*,[35] in which the Tafel slope value of Au nanospheres, Au octahedra and Au nanocubes ranged from 43 mV dec^{-1} to 60 mV dec^{-1}.

One can see that, the ORR activity of the nanocomposite was not only remarkably higher than CNTs alone, but also superior than the direct carbon nanotubes supported samples or similar samples prepared by other approaches. In a recent report by employing bi-metallic Pt–Au nanoparticles supported on multi-wall carbon nanotubes for ORR, the onset potential achieved was only about +0.80 V.[36] The carbon nanotube-gold hybrid materials prepared by Morozan *et al.* demonstrated effective ORR activity in both acidic and basic electrolytes, even if low overpotential requirement was achieved, the number of electron transfer was as low as 3.2.[24]

There are several factors that may contribute to the enhanced activity. First of all, as we employed *in situ* synthetic approach, no surface capping agents of gold nanoparticles were present. The absence of surface ligands and appropriate gold loading in the composite can promote the interfacial charge transfer during the electrochemical reaction.[20,37] Secondly, the integration of carbon nanotubes and gold can provide a synergetic effect on the enhanced ORR activity. Such interaction was evidenced by the Au4f electron binding energy shift observed in XPS measurements. Note that, carbon nanotubes probably not merely serve as a support but also play a critical role in the metal–carbon interactions.[23,38–40] It has postulated that in the gold/carbon hybrid, the defective carbon nanotubes probably can lower the oxygen dissociation energy through accelerating the charge transfer from gold atoms to oxygen molecules.[6]

In addition, the sample preparation was quite simple and straightforward, rather more advantageous than other conventional approaches. For instances, Erikson *et al.* demonstrated the ORR activity of carbon supported gold catalysts with desirable onset potential and kinetic current density, however, the control of the thickness of Au/C-Nafion layer is rather sophiscated and knotty.[41] Carbon nanotube-gold hybrid has been employed as potent catalyst for ORR, however, such hybrid was prepared through layer-by-layer assembly of small gold nanoparticles anchored onto the modified carbon nanotubes.[24] The assembly requires relatively complicated surface functionalization of gold nanoparticles and tedious synthetic procedures while the modification of carbon nanotubes needs cautious chemical conjugation without high yield.[24]

To disclose the physical origin of the higher ORR activity of the Au/CNTs = 1 : 2 sample, the electrochemically active surface area (ECSA) test was conducted.[42,43] Based on the cyclic voltammograms in Fig. S6,† the ECSA value was calculated as 9.45 m^2 g^{-1} for Au/CNTs = 1 : 4, 11.6 m^2 g^{-1} for Au/CNTs = 1 : 2, 2.22 m^2 g^{-1} for Au/CNTs = 1 : 1 and 2.18 m^2 g^{-1} for Au/CNTs = 2 : 1. The sample of Au/CNTs = 1 : 2 possessed the highest ECSA value among the series. Table 1 summarizes the specific activities and mass activities of nanocomposite catalysts as well as commercial Pt/C. One can see that, for Au/CNTs = 1 : 2, even if the mass activity is lower than Pt/C, the specific activity is slightly higher, so a close or comparable activity with Pt/C was acquired.

Finally, the durability of the nanocomposite of Au/CNTs = 1 : 2 was examined by the stability test and compared with

Table 1 The specific activities and mass activities at 0.6 V of Au/CNTs nanocomposites and Pt/C

Sample	Specific activity at 0.6 V (mA cm^{-2})	Mass activity at 0.6 V (mA mg^{-1})
Au/CNTs = 1 : 4	0.29	49.1
Au/CNTs = 1 : 2	0.67	72.5
Au/CNTs = 1 : 1	0.32	16.3
Au/CNTs = 2 : 1	0.3	7.2
Pt/C	0.66	101

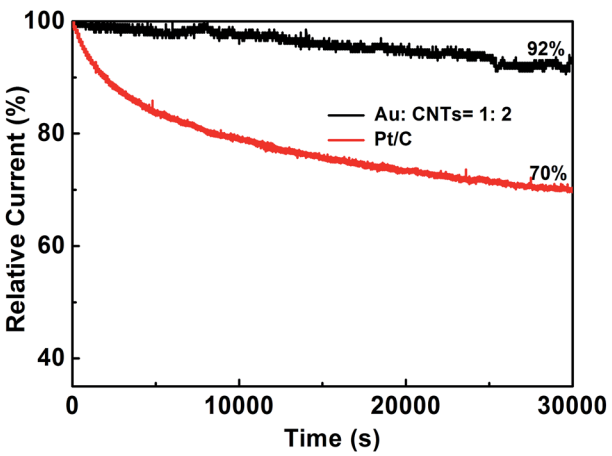

Fig. 5 Chronoamperometric responses for ORR at Au/CNTs = 1 : 2 electrode in an oxygen-saturated 0.1 M KOH solution at +0.5 V for 30 000 s.

commercial Pt/C. As shown in Fig. 5, after more than 8 h's continuous operation, the cathodic current of the nanocomposite electrode only dropped to 92.0%, with a small loss of ~8%. However, the cathodic current of Pt/C electrode dropped to 70%, with a much larger loss of 30%, hence the durability of Au/CNTs (1 : 2) was markedly higher than the commercial Pt/C. Note that the ORR performance of this sample demonstrated great reproducibility, as different batches exhibited almost identical polarization behaviors, further attesting the reliability of the *in situ* approach (Fig. S7†).

Conclusions

In summary, the composite catalysts of Au/CNTs hybrid materials were prepared through a facile *in situ* reduction method and employed as efficient catalysts for oxygen electroreduction. In a series of tested samples, the sample with the mass ratio of Au/CNTs = 1 : 2 possessed the best activity, in terms of onset potential, kinetic current density as well as the number of electron transfer. This sample also demonstrated markedly higher long-term durability than commercial Pt/C. The findings not only highlight the *in situ* method as the green and clean technique with atomic economy, but also provides a useful and effective approach for fabricating other hybrid materials with optimized electrocatalytic activity for ORR.

Acknowledgements

This work was supported by the National Natural Science Foundation of China (No. 21501059 from Z. H. T and No. 51306040 from C. H. W). Z. H. T also acknowledges financial support from Project of Public Interest Research and Capacity Building of Guangdong Province (2015A010105009), Guangdong Innovative and Entrepreneurial Research Team Program (No. 2014 ZT05N200), Guangdong Natural Science Funds for Distinguished Young Scholars (No. 2015A030306006).

References

1 A. Kraytsberg and Y. Ein-Eli, *Energy Fuels*, 2014, **28**, 7303–7330.
2 M. K. Debe, *Nature*, 2012, **486**, 43–51.
3 S. Guo, S. Zhang and S. Sun, *Angew. Chem., Int. Ed.*, 2013, **52**, 8526–8544.
4 Y. Jiao, Y. Zheng, M. Jaroniec and S. Z. Qiao, *Chem. Soc. Rev.*, 2015, **44**, 2060–2086.
5 L. Dai, Y. Xue, L. Qu, H.-J. Choi and J.-B. Baek, *Chem. Rev.*, 2015, **115**, 4823–4892.
6 M. Liu, R. Zhang and W. Chen, *Chem. Rev.*, 2014, **114**, 5117–5160.
7 W. Ding, L. Li, K. Xiong, Y. Wang, W. Li, Y. Nie, S. Chen, X. Qi and Z. Wei, *J. Am. Chem. Soc.*, 2015, **137**, 5414–5420.
8 B. Lim, M. Jiang, P. H. C. Camargo, E. C. Cho, J. Tao, X. Lu, Y. Zhu and Y. Xia, *Science*, 2009, **324**, 1302–1305.
9 G. Wu and P. Zelenay, *Acc. Chem. Res.*, 2013, **46**, 1878–1889.
10 H.-W. Liang, W. Wei, Z.-S. Wu, X. Feng and K. Müllen, *J. Am. Chem. Soc.*, 2013, **135**, 16002–16005.
11 P. Zhang, F. Sun, Z. Xiang, Z. Shen, J. Yun and D. Cao, *Energy Environ. Sci.*, 2014, **7**, 442–450.
12 W. Niu, L. Li, X. Liu, N. Wang, J. Liu, W. Zhou, Z. Tang and S. Chen, *J. Am. Chem. Soc.*, 2015, **137**, 5555–5562.
13 C.-H. Cui and S.-H. Yu, *Acc. Chem. Res.*, 2013, **46**, 1427–1437.
14 X. Huang, Z. Zhao, L. Cao, Y. Chen, E. Zhu, Z. Lin, M. Li, A. Yan, A. Zettl, Y. M. Wang, X. Duan, T. Mueller and Y. Huang, *Science*, 2015, **348**, 1230–1234.
15 D. Grumelli, B. Wurster, S. Stepanow and K. Kern, *Nat. Commun.*, 2013, **4**, 2904–2909.
16 G. Li and R. Jin, *Acc. Chem. Res.*, 2013, **46**, 1749–1758.
17 W. Chen and S. Chen, *Angew. Chem., Int. Ed.*, 2009, **48**, 4386–4389.
18 Y. Lu and W. Chen, *Chem. Soc. Rev.*, 2012, **41**, 3594–3623.
19 H. Hakkinen, *Chem. Soc. Rev.*, 2008, **37**, 1847–1859.
20 D. Li, C. Wang, D. Tripkovic, S. Sun, N. M. Markovic and V. R. Stamenkovic, *ACS Catal.*, 2012, **2**, 1358–1362.
21 C. Jeyabharathi, S. Senthil Kumar, G. V. M. Kiruthika and K. L. N. Phani, *Angew. Chem., Int. Ed.*, 2010, **49**, 2925–2928.
22 L. Wang, Z. Tang, X. Liu, W. Niu, K. Zhou, H. Yang, W. Zhou, L. Li and S. Chen, *RSC Adv.*, 2015, **5**, 103421–103427.
23 Q. Wang, L. Wang, Z. Tang, F. Wang, W. Yan, H. Yang, W. Zhou, L. Li, X. Kang and S. Chen, *Nanoscale*, 2016, **8**, 6629–6635.
24 A. Morozan, S. Donck, V. Artero, E. Gravel and E. Doris, *Nanoscale*, 2015, **7**, 17274–17277.
25 C. Lin, Y. Song, L. Cao and S. Chen, *ACS Appl. Mater. Interfaces*, 2013, **5**, 13305–13311.
26 W. Chen, D. Ny and S. Chen, *J. Power Sources*, 2010, **195**, 412–418.
27 N. Alexeyeva, T. Laaksonen, K. Kontturi, F. Mirkhalaf, D. J. Schiffrin and K. Tammeveski, *Electrochem. Commun.*, 2006, **8**, 1475–1480.
28 N. Alexeyeva and K. Tammeveski, *Anal. Chim. Acta*, 2008, **618**, 140–146.
29 N. Alexeyeva, J. Kozlova, V. Sammelselg, P. Ritslaid, H. Mändar and K. Tammeveski, *Appl. Surf. Sci.*, 2010, **256**, 3040–3046.
30 H. Yin, H. Tang, D. Wang, Y. Gao and Z. Tang, *ACS Nano*, 2012, **6**, 8288–8297.
31 H. Qian and R. Jin, *Nano Lett.*, 2009, **9**, 4083–4087.
32 A. J. Bard and L. R. Faulkner, *Electrochemical Methods: Fundamentals and Applications*, Wiley, New York, 2nd edn, 2001, p. 341.
33 C. Wang, N. M. Markovic and V. R. Stamenkovic, *ACS Catal.*, 2012, **2**, 891–898.
34 N. Ramaswamy and S. Mukerjee, *Adv. Phys. Chem.*, 2012, **2012**, 1–17.
35 H. Erikson, A. Sarapuu, K. Tammeveski, J. Solla-Gullón and J. M. Feliu, *ChemElectroChem*, 2014, **1**, 1338–1347.
36 R. M. Félix-Navarro, M. Beltrán-Gastélum, E. A. Reynoso-Soto, F. Paraguay-Delgado, G. Alonso-Nuñez and J. R. Flores-Hernández, *Renewable Energy*, 2016, **87**, 31–41.
37 Y. Lee, A. Loew and S. Sun, *Chem. Mater.*, 2010, **22**, 755–761.
38 D. A. Slanac, A. Lie, J. A. Paulson, K. J. Stevenson and K. P. Johnston, *J. Phys. Chem. C*, 2012, **116**, 11032–11039.

39 D. A. Slanac, W. G. Hardin, K. P. Johnston and K. J. Stevenson, *J. Am. Chem. Soc.*, 2012, **134**, 9812–9819.
40 C. P. Deming, R. Mercado, V. Gadiraju, S. W. Sweeney, M. Khan and S. Chen, *ACS Sustainable Chem. Eng.*, 2015, **3**, 3315–3323.
41 H. Erikson, G. Jürmann, A. Sarapuu, R. J. Potter and K. Tammeveski, *Electrochim. Acta*, 2009, **54**, 7483–7489.
42 Y. Li, W. Gao, L. Ci, C. Wang and P. M. Ajayan, *Carbon*, 2010, **48**, 1124–1130.
43 E. Higuchi, K. Hayashi, M. Chiku and H. Inoue, *Electrocatalysis*, 2012, **3**, 274–283.